Electrodeposited Nanoporous PtY Alloy Electrodes with Enhanced Oxygen Reduction Reaction

Sang-Beom Han, Da-Hee Kwak, Young-Woo Lee, Si-Jin Kim, Jin-Yeon Lee, Seul Lee, Hye-Jin Kwon, and Kyung-Won Park[*]

Department of Chemical Engineering, Soongsil University, Seoul 156-743, Korea
[*]E-mail: kwpark@ssu.ac.kr

Pt-based alloy nanostructures are known to exhibit improved electrocatalytic properties due to their particularly modulated surface and electronic structures favourable for oxygen reduction reactions. Here, we report nanoporous PtY alloy electrodes fabricated using electrodeposition method at a high reduction potential in anhydrous metal salt solutions. The as-deposited PtY electrodes show a nanoporous well-defined alloy nanostructure via transmission electron microscopy and X-ray diffraction methods. The PtY alloy electrodes exhibit enhanced electrochemical activity for ORR, i.e. higher specific current and half-wave potential in ORR compared with a conventional Pt electrocatalyst. The improved electrochemical activity of the electrodeposited PtY electrodes in ORR is ascribed to the nanoporous structure and alloy surface due to the Y atoms in the alloy phase.

Keywords: Nanoporous, Platinum, Yttrium, Alloy, Electrodeposition, Oxygen reduction reaction

1. INTRODUCTION

Oxygen reduction reaction (ORR) is well known as the most important reaction in biological respiration and energy converting systems such as fuel cells.[1-3] Especially, in proton exchange membrane fuel cells (PEMFCs), the ORR at the cathode exhibits very slow kinetics, responsible for polarization losses of over 0.3-0.4 V under typical operation conditions.[4-6] The deteriorated electrochemical reduction of the oxygen as an oxidant can result in a much higher amount of loading of Pt-based noble metal catalysts in comparison with fast hydrogen oxidation at the anode in the PEMFCs. [7-9] Many researchers have therefore focused on enhanced electrocatalytic properties in ORR through crystal plane- or size-control and alloy formation in ORR catalysts.[10-13]

Recent works on the crystal surface control of Pt-based nanoparticles and alloy structure with transition metals have been carried out to increase the ORR activity. Markovic et al. demonstrated that

the order of the ORR activity of different crystal planes in the various single-crystals in perchloric acid electrolyte was as follows: Pt(110) > Pt(111) > Pt(100).[14,15] Several Pt alloys, including late transition metals such as Ni, Co, Cr and Fe, and rare earth transition metals such as Sc and Y, have been reported as promising ORR electro-catalysts.[16-19] Among these Pt-based alloy catalysts, PtY is a promising candidate with an excellent catalytic activity for ORR.[20-23] However, the chemical synthesis of PtY alloys is extremely difficult due to the relatively low standard reduction potential of yttrium (-2.37 V vs. NHE) compared with platinum (0.755 V. vs. NHE).[24-26]

It has been reported that the electrochemical characteristics of electrode materials are highly dependent on the size, surface area, and morphology of the material. Electrochemical characteristics can be enhanced by controlling the nanostructures of the electrode material.[27,28] In order to control the size of electrode materials, many chemical approaches have been suggested for the preparation of highly dispersed metal clusters while controlling the size, such as the impregnation of the carbon support with suitable metal salts. Among these approaches, the electrodeposition technique was found to be an effective method for the preparation of nanostructures because of its simple operation, high purity, and easy control of the size.[29-31] Here, PtY alloy nanostructure electrodes were prepared using the electrodeposition method in an anhydrous alcohol solution. The PtY alloy nanostructures were characterized using scanning electron microscopy (SEM), transmission electron microscopy (TEM), X-ray diffraction (XRD). To investigate the electrochemical properties and catalytic activity of the samples, cyclic voltammetry (CVs) and linear scanning voltammetry of the electrodes were carried out using a potentiostat.

2. EXPERIMENTAL

2.1 Preperation of Electrode

Electrodeposition on a rotating glassy carbon electrode as a substrate was carried out in an anhydrous ethanol solution containing H_2PtCl_6 (6 mM) and YCl_3 (5, 10, and 15 mM; denoted as PtY-05, PtY-10, and PtY15, repectively). A Pt mesh and Ag/AgCl were used as a counter and a reference electrode, respectively. An overpotential of -4.3 V *vs.* reversible hydrogen electrode (RHE) was applied with a rotating speed of 1000 rpm for 1500 s in order to nucleate and grow the electrodes. The electrodes were then kept at -1.3 V *vs*. RHE for 100 s in the solution at room temperature.

2.2 Materials characterization

The morphology of the as-prepared PtY electrodes was observed using SEM (JEOL JSM-6360A) and TEM (JEOL JEM-ARM 200F) analysis. The TEM investigation was carried out at an accelerating voltage of 200 kV and Cu grids were used as substrates. The crystal structure of the PtY electrodes was confirmed using thin-film XRD (Rigaku D/MAX-2500) equipped with a Cu K_α source. The XRD analysis was carried out using a Rigaku X-ray diffractometer with a Cu K_α ($\lambda = 0.15418$ nm) source with a Ni filter.

2.3 Electrochemical measurement

To evaluate the electrochemical properties and catalytic activity of the PtY electrodes, CVs were obtained in 0.1 M HClO$_4$ with a scan rate of 50 mV s^{-1} at 25 ^{o}C. The electrochemical properties of the samples were measured in a three-electrode cell at 25 ^{o}C using a potentiostat (Eco Chemie, AUTOLAB). The glassy carbon electrode as a working electrode was polished using 1, 0.3, and 0.05 μm Al$_2$O$_3$ paste and then washed in deionized water. Pt wire and Ag/AgCl (in saturated KCl) were used as a counter and reference electrode, respectively. All potentials are reported with respect to RHE. The electrochemical active surface areas (EASAs) of the PtY electrodes were measured by integrating hydrogen desorption regions (assuming 210 μC cm^{-2} of polycrystalline Pt electrode) in 0.1 M HClO$_4$. The oxygen reduction current–potential curves were obtained using linear sweep voltammetry (LSV) at a rotation speed of 1600 rpm in O$_2$-saturated 0.1M HClO$_4$ by sweeping potential from 1.1 to 0.3 V vs. RHE with a scan rate of 5 mV s^{-1}. The stability test was carried out by applying linear potential sweeps for 3000 cycles between 0.4 and 0.9 V at a scan rate of 50 mV s^{-1} in O$_2$-saturated 0.1 M HClO$_4$ solution at 25 ^{o}C. To compare properties of the catalysts after the durability test, the oxygen reduction current-potential curves of the catalysts after the stability test were obtained by sweeping the potential from 1.1 to 0.3 V at a scan rate of 5 mV s^{-1} and rotation disk speed of 1600 rpm.

3. RESULTS AND DISCUSSION

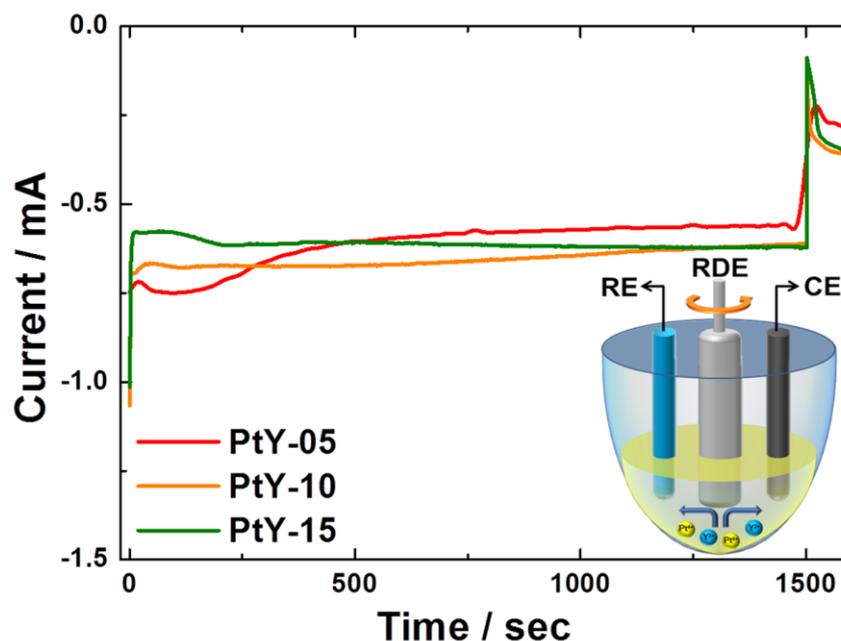**Figure 1**. Electrodeposition on a rotating glassy carbon electrode as a substrate was carried out in an anhydrous ethanol solution containing H$_2$PtCl$_6$(6 mM) and YCl$_3$(5, 10, and 15 mM). Pt mesh and Ag/AgCl were used as a counter and a reference electrode, respectively.

The PtY electrodes were prepared through electrodeposition on glassy carbon electrodes with a rotation rate of 1,000 rpm in anhydrous metal salt solutions. As shown in Figure 1, the reduction current decreased as the concentration of yttrium salt increased from 5 to 15 mM.
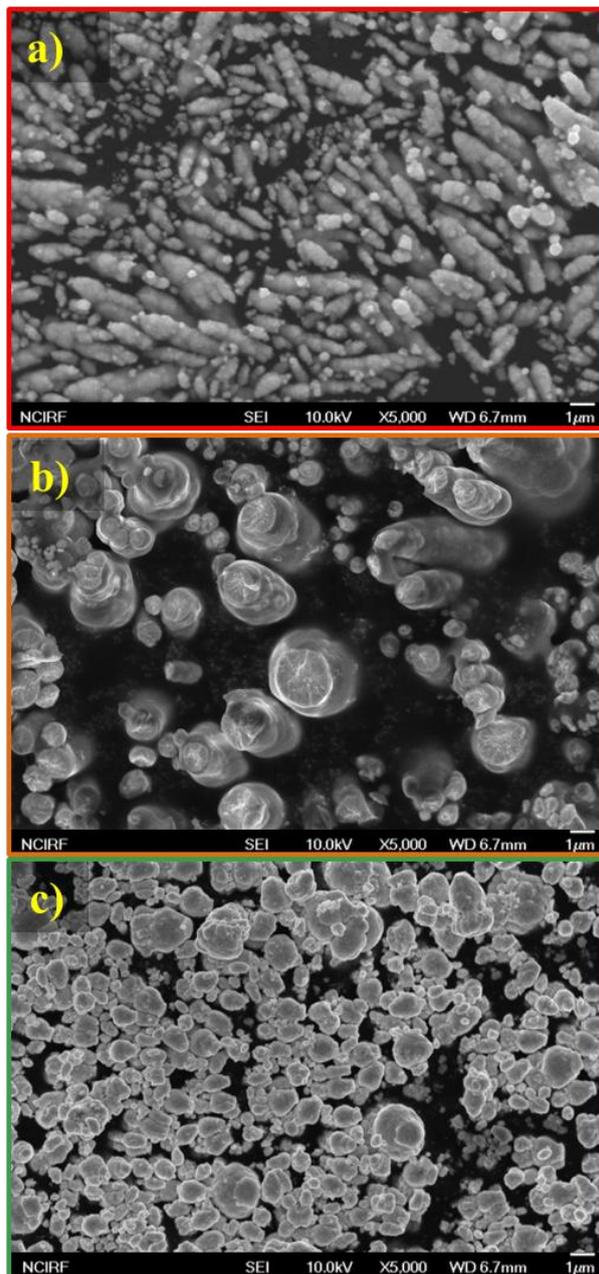
Figure 2. SEM images of (a) PtY-05, (b) PtY-10, and (c) PtY-15 electrodes prepared via the electrodeposition method with different concentrations of yttrium salt.

The SEM images of PtY electrodes prepared via the electrodeposition method with different concentrations of yttrium salt (denoted as PtY-05, PtY-10, and PtY-15, respectively) are shown in Figure 2. The PtY-05 and PtY-10 exhibited free-standing rod shapes with lengths of 0.5-1 μm and 1-3 μm, respectively. The PtY-05 showed a rod with a smaller diameter than that of PtY-10, due to an increased nucleation rate with a high initial reduction current during the electrodeposition process. In contrast, the PtY-15 exhibited a spherical shape, rather than a rod shape, due to a relatively slow growth rate, i.e. a low reduction current for the electrodeposition.
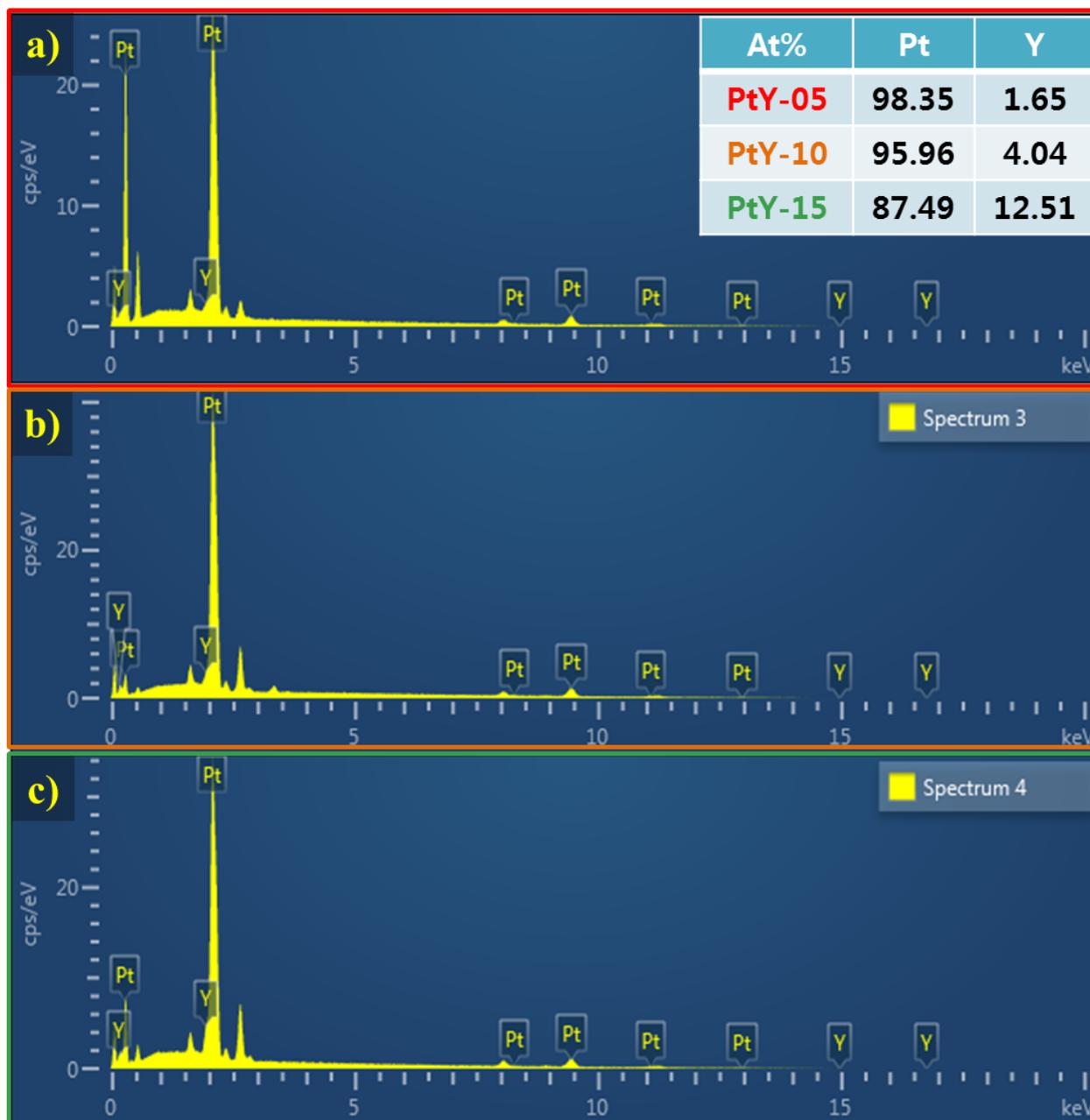
At%	Pt	Y
PtY-05	98.35	1.65
PtY-10	95.96	4.04
PtY-15	87.49	12.51

Figure 3. EDX spectra of (a) PtY-05, (b) PtY-10, and (c) PtY-15 electrodes prepared via the electrodeposition method with different concentrations of yttrium salt.

The bulk composition of the as-prepared PtY electrodes was investigated using energy dispersive X-ray spectroscopy (EDX), as shown in Figure 3. The contents of yttrium for the PtY-05, PtY-10, and PtY-15 were ~1.65, ~4.04, and ~12.51 at%, respectively. Furthermore, the HR-TEM images of the resulting electrodeposited PtY electrodes showed a nanoporous structure with a pore diameter of 1.5-2.5 nm, resulting from a continuous connection of nanoparticles with an average size of 2-4 nm (Figure. 4).
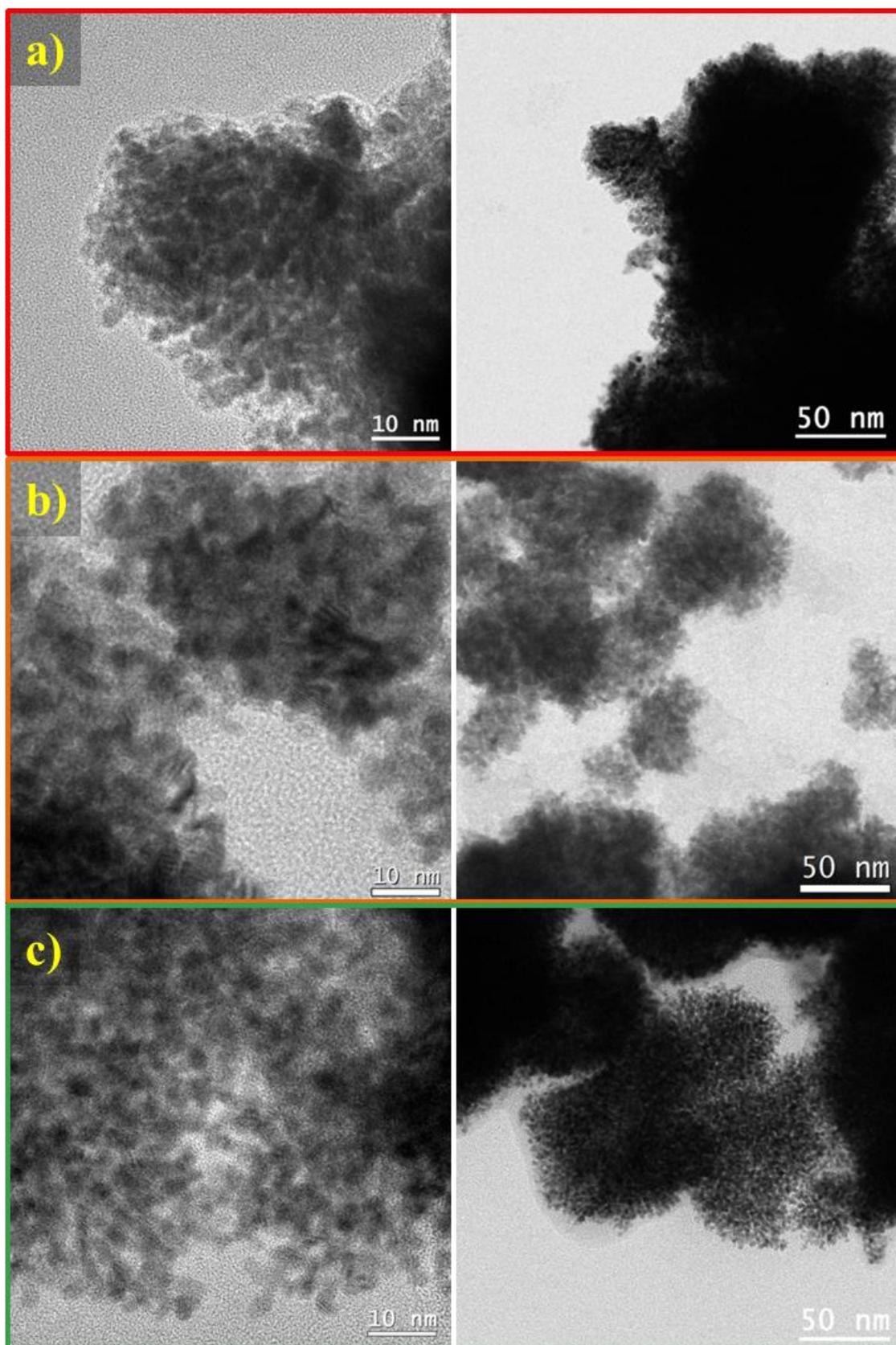
Figure 4. TEM images of (a) PtY-05, (b) PtY-10, and (c) PtY-15 electrodes prepared via the electrodeposition method with different concentrations of yttrium salt.
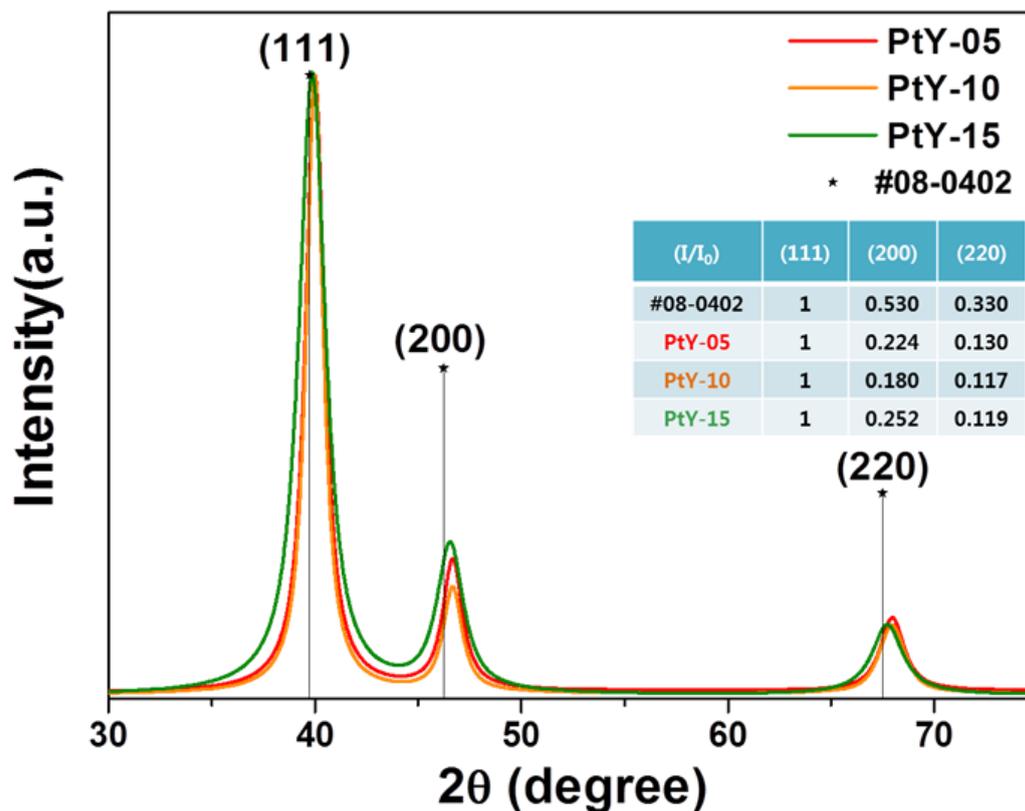
(I/I_0)	(111)	(200)	(220)
#08-0402	1	0.530	0.330
PtY-05	1	0.224	0.130
PtY-10	1	0.180	0.117
PtY-15	1	0.252	0.119

Figure 5. XRD patterns of PtY-05, PtY-10, and PtY-15.

The as-prepared PtY electrodes showed a face-centered cubic (fcc) structure (PDF 08-0402) containing (111), (200), and (220) planes, as shown in the XRD patterns of Figure 5. Typically, the relative intensity ratios of (111) to (200) and (111) to (220) were 0.53 and 0.33, respectively. On the other hand, PtY-05, PtY-10, and PtY-15 exhibited much lower intensity ratios than the reference data of Pt, suggesting that the Pt crystal structures in the PtY electrodes were dominantly oriented in the [111] direction perpendicular to the glassy carbon. As a result, all PtY electrodes contained the (111) texture as a dominant crystal plane, compared with a typical Pt electrode. Assuming a substitutional solid solution between metallic phases, a higher angle shift of the XRD peaks means a well-defined alloy formation between Pt and Y. It has been reported that according to the thermodynamic approach, Pt-based binary alloys such as PtY at ORR activity are superior to pure Pt when using density function theory calculation. The alloying Pt can decrease the overpotential for the electroreduction of HO_{ads} to H_2O by weakening the binding to HO_{ads}.

The surface crystal planes, which can be those involved in the electrochemical reactions, were investigated using the CVs of the electrodes. It should also be noted that, in the case of the PtY electrodes, (111) is believed to be the energetically preferred plane formed in the present electrodeposition condition [32-34].
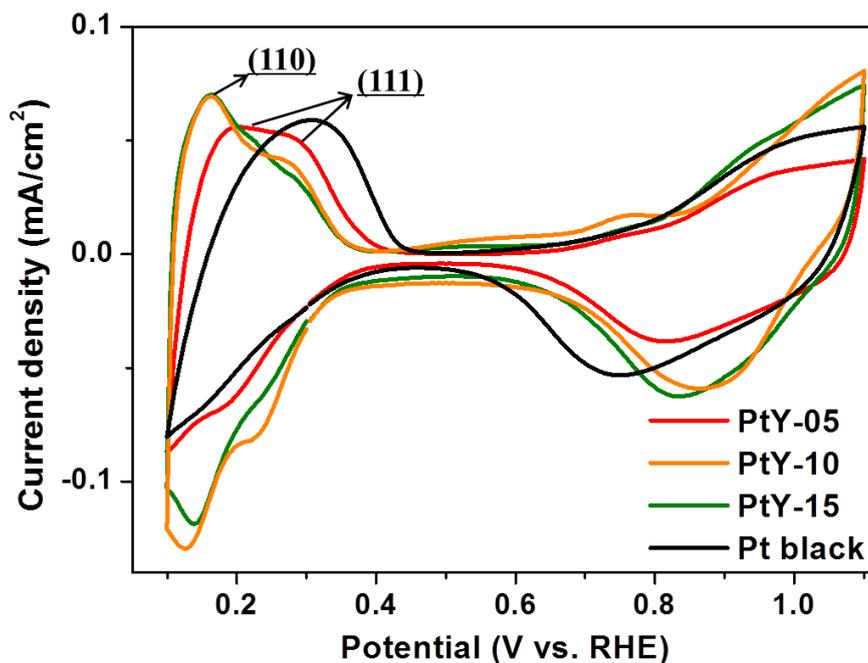
Figure 6. CVs of the PtY electrodes in Ar-saturated 0.1 M HClO$_4$ with a scan rate of 50 mV s^{-1}.

Figure. 6 shows the typical CVs of the PtY electrodes in Ar-saturated 0.1 M HClO$_4$, compared with Pt black as a cathode catalyst. The EASAs of the electrodes were calculated from the area of hydrogen desorption on Pt after subtracting the contribution of the double layer charge using the factor of 210 μC cm^{-2}. From the hydrogen adsorption on Pt, the roughness factor (R$_f$) of the electrodes is defined as a value of EASA divided by the geometric area of the glassy carbon electrode. The values of R$_f$ for PtY-05, PtY-10, PtY-15, and Pt black are 123.4, 147.9, 7.6, and 14.6, respectively. In particular, the roughness factor of R$_f$ for PtY-10 is about 10 times higher than that of Pt black. It appears that this may be attributed to a well-defined nanoporous structure in a rod shape consisting of PtY alloy nanoparticles deposited under a high reduction potential of -4.3 V vs. RHE (Figure 1). It was reported that the nanoporous structure had higher oxygen solubility than the exterior aqueous phase.[9] In the structure, oxygen diffusing into the pores would be chemically biased to remain there. Thus, the frequency of interaction with the surface could be greatly increased within an electrode pore diameter of 1.5-2.5 nm. Furthermore, the PtY alloy electrodes exhibit much higher oxygen reduction peak potentials (0.818-0.864 V) than Pt black (0.750 V). Ross reported the ORR activity on the low-index planes by measuring in a narrow and positive potential region, which may have caused partial disorder of the low-index planes by oxide formation.[35] In particular, Markovic et al. observed that the ORR activity in 0.1 M HClO$_4$ decreases in the order of (110) > (111) > (100).[36] The PtY-05 exhibited hydrogen oxidations at 0.15-0.28 V corresponding to a characteristic peak on the (111) surface. However, the PtY-10 and PtY-15 revealed hydrogen oxidation peaks at ~0.15 V corresponding to a characteristic peak (110) surface as well as (111) surface.
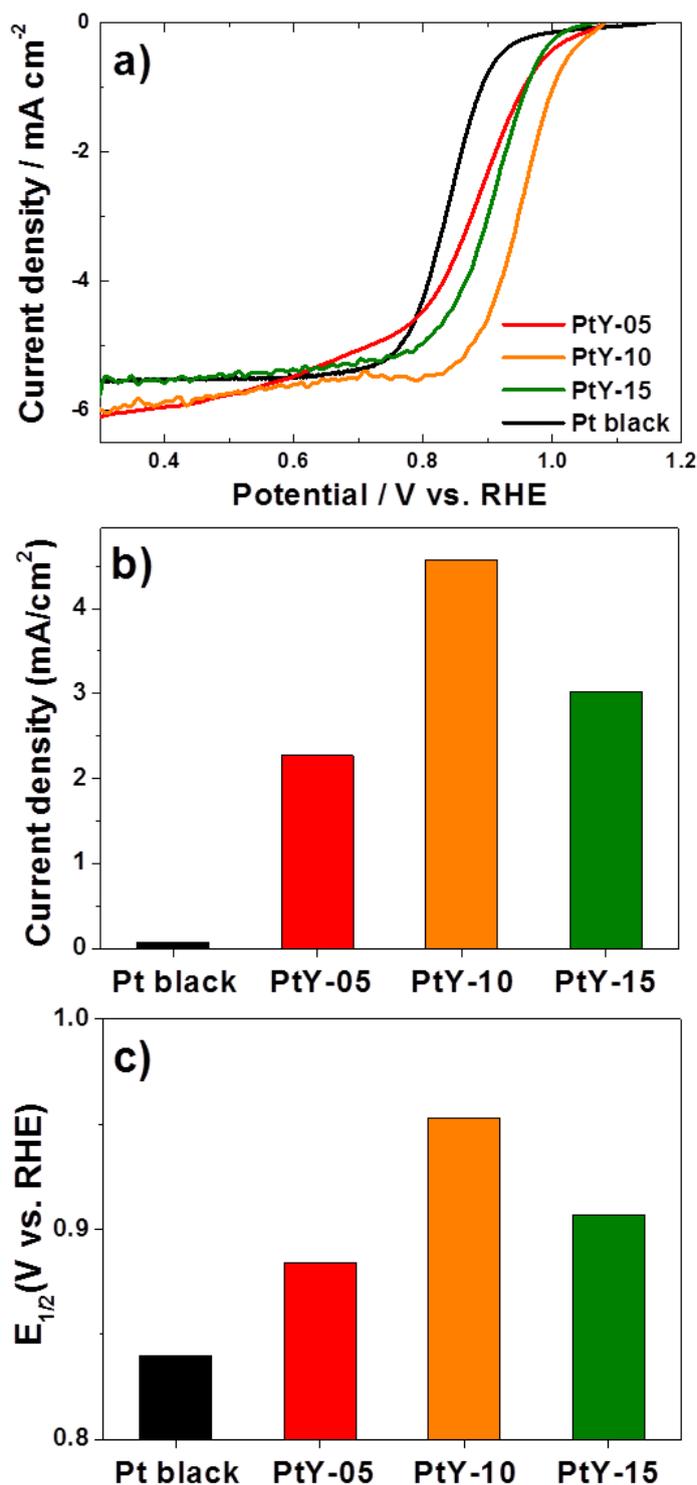
Figure 7. a) Polarization curves of the electrodes for ORR measured between 1.1 and 0.3 V in O_2-saturated 0.1 M $HClO_4$ with a scan rate of 5 mV s^{-1}. b) ORR current densities of the electrodes at 0.9 V. c) Half-wave potentials of the electrodes.

To further compare the ORR performance of the electrodes, the electrocatalytic activity of the PtY electrodes for ORR was measured from 1.1 to 0.3 V in O_2-saturated 0.1 M $HClO_4$ with a scan rate of 5 mV s^{-1}, as shown in Figure 7(a). The ORR current densities of the PtY-05, PtY-10, PtY-15, and Pt

black catalysts at 0.9 V are 2.27, 4.58, 3.02, and 0.078 mA cm^{-2}, respectively (Figure 7(b)). The half-wave potentials of nanoporous PtY-05, PtY-10, PtY-15, and Pt black catalyst are 0.884, 0.953, 0.907, and 0.840 V, respectively (Figure 7(c)). Furthermore, the stability test of the ORR was performed by applying linear potential sweeps between 0.4 and 0.9 V in O$_2$-saturated 0.1 M HClO$_4$ solution at 25 $^{\circ}$C.
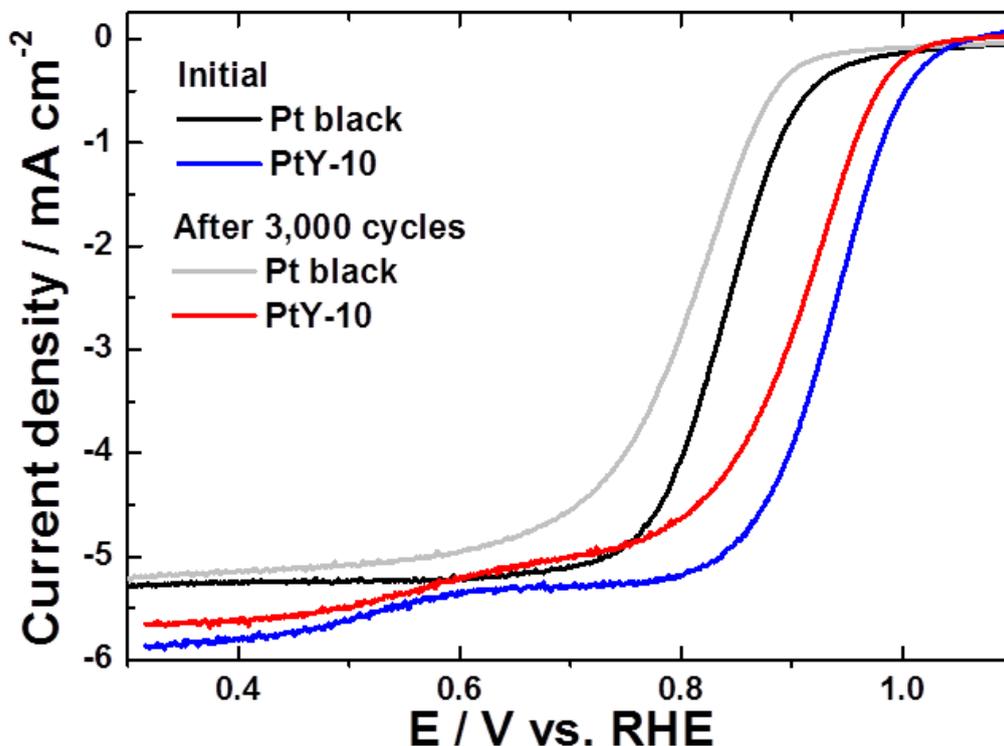

Figure 8. Polarization curves of the electrodes for ORR before and after the stability test between 1.1 and 0.3 V in O$_2$-saturated 0.1 M HClO$_4$ with a scan rate of 5 mV s^{-1}.

After the stability test, the ORR activity of the PtY-10 is still higher than the Pt black catalyst, as shown in Fig. 8. As a result, the nanoporous PtY alloy electrodes exhibit much enhanced ORR performance, i.e. high kinetic current densities, improved half-wave potentials, and enhanced stability. In particular, Y in the PtY alloy electrodes exhibits much enhanced ORR activity by lowering the blocking effect of O$_2$, O/OH, O^{2-}, and H$_2$O$_2$. Furthermore, the nanoporous structure of the PtY alloy electrodes, which can be formed at a high reduction potential, might increase the frequency of the interaction with the electrode surface with oxygen molecules, leading to an improved performance in the ORR.

4. CONCLUSIONS

In summary, nanoporous PtY alloy electrodes were fabricated using electrodeposition method at a high reduction potential in an anhydrous ethanol solution. The PtY electrodes formed a nanoporous structure consisting of PtY alloy nanophases with small grain size. The improved ORR activity and stability of nanoporous PtY alloy electrodes formed at a high reduction potential could be

attributed to the nanoporous alloy structure, thus increasing the frequency of the interaction with the electrode surface with oxygen molecules.

References

1. J. P. Collman, T. Kodadek, S. A. Raybuck , J. I. Brauman and L.M. Papazian, *J. Am. Chem. Soc.*, 107 (1985) 4343.
2. J. P. Collman, J. I. Brauman and K. S. Suslick, *J. Am. Chem. Soc.*, 97 (1975) 7185.
3. R. Bashyam and P. Zelenay, *Nature*, 443 (2006) 63.
4. T. Toda, H. Igarashi, H. Uchida and M. Watanabe, *J. Electrochem. Soc.*, 146 (1999) 3750.
5. J. K. Nørskov, J. Rossmeisl, A. Logadottir, L. Lindqvist, J. R. Kitchin, T. Bligaard and H. Jónsson, *J. Phys. Chem. B*, 108 (2004) 17886.
6. S. J. Hwang, S. -J. Yoo, S. Jang, T. -H. Lim, S. A. Hong and S.-K. Kim, *J. Phys. Chem. C*, 115 (2011) 2483.
7. S. Gamburzev and A. J. Appleby, *J. Power Sources*, 107 (2002) 5.
8. V. Celorrio, J. J. Flóez-Montaño, R. Moliner, E. Pastor and M. J. Lázaro, *Int. J. Hydrogen Energy*, 39 (2014) 5371.
9. L. Krishnan, G. Yeager, K. Clark, J. Kerr and G. Soloveichik, *Fuel Cells*, 1 (2015) 239.
10. J. Zhang, H. Yang, Y. Fang and S. Zou, *Nano Lett.*, 10 (2010) 638.
11. C. Wang, H. Daimon, Y. Lee, J. Kim and S. Sun, *J. Am. Chem. Soc.*, 129 (2007) 6974.
12. Y. Kang, J. B. Pyo, X. Ye, R. E. Diaz, T. R. Gordon, E. A. Stach and C. B. Murray, *ACS Nano*, 7 (2013) 645.
13. Y. -W Lee, A. -R. Ko, D. -Y. Kim, S. -B. Han and K. -W. Park, *RSC Adv.*, 2 (2012) 1119.
14. N. M. Marković, H. A. Gasteiger and P. N. Ross Jr., *J. Phys. Chem.*, 99 (1995) 3411.
15. V. Stamenkovic, N. M. Marković and P. N. Ross Jr., *J. Electroanal. Chem.*, 500 (2001) 44.
16. N. N. Kariuki, W. J. Khudhayer, T. Karabacak and D. J. Myers, *ACS Catal.*, 3 (2013) 3123.
17. C. Wang, N. M. Markovic and V. R. Stamenkovic, *ACS Catal.*, 2 (2012) 891.
18. M. K. Jeon and P. J. McGinn, *J. Power Sources*, 196 (2011) 1127.
19. C. Koenigsmann, A. C. Santulli, K. Gong, M. B. Vukmirovic, W. -P. Zhou, E. Sutter, S. S. Wong and R. R. Adzic, *J. Am. Chem. Soc.*, 133 (2011) 9783.
20. J. Greeley, I. E. L. Stephens, A. S. Bondarenko, T. P. Johansson, H. A. Hansen, T. F. Jaramillo, J. Rossmeisl, I. Chorkendorff and J. K. Nørskov, *Nature Chem.*, 1 (2009) 552.
21. P. Hernandez-Fernandez, F. Masini, D. N.McCarthy, C. E. Strebel, D. Friebel, D. Deiana, P. Malacrida, A. Nierhoff, A. Bodin, A. M. Wise, J. H. Nielsen, T. W. Hansen, A. Nilsson, I. E. L. Stephens and I. Chorkendorff, *Nature Chem.*, 6 (2014) 732.
22. S. J. Yoo, S. -K. Kim, T. -Y. Jeon, S. J. Hwang, J.-G. Lee, S. -C. Lee, K. -S. Lee, Y. -H. Cho, Y. -E. Sung and T. -H. Lim, *Chem. Commun.*, 47 (2011) 11414.
23. K. G. Nishanth, P. Sridhar and S. Pitchumani, *Electrochem. Commun.*, 13 (2011) 1465.
24. G. Milazzo, S. Caroli and V. K. Sharma, Tables of Standard Electrode Potentials, Wiley, Chichester, 1978.
25. J. Bard, R. Parsons and J. Jordan, Standard Potentials in Aqueous Solutions, Marcel Dekker, New York, 1985.
26. S. G. Bratsch, *J. Phys. Chem. Ref. Data*, 18 (1989) 1.

27. J. Snyder, T. Fujita, M. W. Chen and J. Erlebacher, *Nature Mater.*, 9 (2010) 904.
28. V. R. Stamenkovic, B. Fowler, B. S. Mun, G. Wang, P. N. Ross, C. A. Lucas and N. M. Marković, *Science*, 315 (2007) 493.
29. L. Cunci, C. A. Velez, I. Perez, A. Suleiman, E. Larios, M. José-Yacamán, J. J. Watkins and C. R. Cabrera, *ACS Appl. Mater. Interfaces*, 6 (2014) 2137.
30. L. M. Glukhov, A. A. Greish and L. M. Kustov, *Russ. J. Phys. Chem.*, 84 (2010) 104.
31. Y. –J. Song, J. –K. Oh, K. –W. Park, *Nanotechnology*, 19 (2008) 355602.
32. T. Aaltonen, M. Ritala, T. Sajavaara, J. Keinonen and M. Leskelä, *Chem. Mater.*, 15 (2003) 1924.
33. R. Huang, Y. –H. Wen, Z. –Z. Zhu and S. –G. Sun, *J. Mater. Chem.*, 21 (2011) 11578.
34. W. H. Lee, K. R. Vanloon, V. Petrova, J. B. Woodhouse, C. M. Loxton and R. I. Masel, *J. Catal.*, 126 (1990) 658.
35. P. N. Ross Jr. *J. Electrochem. Soc.*, 126 (1979) 78.
36. N.M. Marković, R.R. Adžić, B.D. Cahan and E.B. Yeager, *J. Electroanal. Chem.*, 377 (1994) 249.